Supplemental Material to "Lift induced by slip inhomogeneities in lubricated contacts"

Aidan Rinehart[1], Uğis Lācis[1], Thomas Salez[2,3], and Shervin Bagheri[1*]
[1] *Department of Mechanics, KTH Royal Institute of Technology, Stockholm 11428, SE*
[2] *Univ. Bordeaux, CNRS, LOMA, UMR 5798, F-33405, Talence, France. and*
[3] *Global Station for Soft Matter, Global Institution for Collaborative Research and Education, Hokkaido University, Sapporo, Hokkaido 060-0808, Japan.*
(Dated: Nobember 2019)

In this material we provide more detailed analytical derivations of lubrication forces in sections I and II. In section III we provide Taylor expansions of force coefficients needed for displacement scaling estimates and the details of scaling law derivations. Then, in section IV we discuss a correction of the single transition scaling law that allows to capture the net migration away from the patterned wall. Finally, in section V we provide details of the numerical method used for producing the particle trajectories.

I. ANALYTICAL DERIVATIONS OF FORCES AND RESISTANCE COEFFICIENTS

In the following we provide some detailed derivations for the analytical expressions and scaling arguments provided in the main text. We begin with the forces and torques generated by the fluid resisting the motion of the cylinder,

$$\boldsymbol{F} = \int_S \boldsymbol{\sigma}\cdot\boldsymbol{n}\mathrm{d}S, \qquad\qquad T = \int_S \boldsymbol{r}\times(\boldsymbol{\sigma}\cdot\boldsymbol{n})\mathrm{d}S. \tag{S1}$$

Here, S is the cylinder surface, $\boldsymbol{\sigma}$ is the fluid stress tensor, $\boldsymbol{n}$ the surface normal vector, and $\boldsymbol{r}$ the cylinder radius. The forces and torques expressed in terms of the flow velocities, u, w and pressure p are as follows,

$$F_x = \int_S \left(-p + 2\eta\frac{\partial u}{\partial x}\right)n_x + \eta\left(\frac{\partial u}{\partial z}+\frac{\partial w}{\partial x}\right)n_z\mathrm{d}S, \quad F_z = \int_S \left(-p + 2\eta\frac{\partial w}{\partial z}\right)n_z + \eta\left(\frac{\partial u}{\partial z}+\frac{\partial w}{\partial x}\right)n_x\mathrm{d}S, \tag{S2}$$

$$T = r\int_S 2\eta\left(\frac{\partial w}{\partial z}-\frac{\partial u}{\partial x}\right)n_x n_z + \eta\left(\frac{\partial u}{\partial z}+\frac{\partial w}{\partial x}\right)(n_x^2-n_z^2)\mathrm{d}S. \tag{S3}$$

We proceed with the exact derivations of the force and torques for the three modes of motion; wall parallel, wall normal and rotation, additionally showing that the resistance matrix obtains the expected symmetric form.

I.1. Wall Parallel and Rotation Motion

The wall parallel and rotation motions share the non-dimensional relationships obtained from the standard lubrication scaling given in the main text. The following derivation also requires the non-dimensional unit normal vector $\boldsymbol{N} = [\sqrt{2}\varepsilon^{1/2}X\hat{e}_x, -\hat{e}_z]$. Introduction of these non-dimensional variables into the Eqs. S2-S3 provide force and torque expressions with the scale separation parameter, $\varepsilon = \delta_0/r$. Application of the lubrication scaling to Eq. S2 gives,

$$F_x = \int_{-\infty}^{\infty}\left(-\sqrt{2}\eta V\varepsilon^{-1/2}XP + 2\sqrt{2}\eta V\varepsilon^{1/2}X\frac{\partial U}{\partial X}\right) - \eta\left(\sqrt{2}\varepsilon^{-1/2}V\frac{\partial U}{\partial Z}+\varepsilon^{1/2}\frac{\partial W}{\partial X}\right)\mathrm{d}X. \tag{S4}$$

The leading order terms of the non-dimensional integral are grouped into the leading order expression,

$$F_x = -\sqrt{2}\eta V\varepsilon^{-1/2}\int_{-\infty}^{\infty} 2XP + \frac{\partial U}{\partial Z}\mathrm{d}X. \tag{S5}$$

This is the form we report in the main text Eq. 4, with viscosity and velocity scaled out consistent with resistance matrix notation. Moving to the force along the z-axis one obtains,

$$F_z = \int_{-\infty}^{\infty}\left(2\eta V\varepsilon^{-1}P - 2\sqrt{2}\frac{\partial W}{\partial Z}\right) + \eta\left(2V\frac{\partial U}{\partial Z}+\sqrt{2}V\frac{\partial W}{\partial X}\right)X\mathrm{d}X. \tag{S6}$$

* corresponding author: shervin@mech.kth.se

Considering only the leading order terms of ε one obtains,

$$F_z = 2\eta V \varepsilon^{-1} \int_{-\infty}^{\infty} P \mathrm{d}X. \tag{S7}$$

This is the wall normal force form presented in the main text Eq. 5, with viscosity and velocity factored out. Finally torque for wall parallel motion and rotation takes the form,

$$T = r\eta V \int_{-\infty}^{\infty} -2\sqrt{2}\varepsilon^{1/2} X \left(\frac{\partial U}{\partial X} + \frac{\partial W}{\partial Z}\right) - \sqrt{2}\left(\varepsilon^{-1/2}\frac{\partial U}{\partial Z} + \frac{\varepsilon^{1/2}}{2}\frac{\partial W}{\partial X}\right) - 2X^2\left(\sqrt{2}\varepsilon^{1/2}\frac{\partial U}{\partial Z} + \varepsilon^{3/2}\frac{\partial W}{\partial X}\right)\mathrm{d}X. \tag{S8}$$

Lastly we obtain Eq. S9 the leading order equation for torque presented in the main text as Eq. 5,

$$T = -\sqrt{2}\eta V \varepsilon^{-1/2} r \int_{-\infty}^{\infty} \frac{\partial U}{\partial Z}\mathrm{d}X. \tag{S9}$$

One can note the different powers of ε^{α} where F_x and T have $\alpha = -1/2$ and F_z has $\alpha = -1$. Consequently the magnitude of these forces and torques will grow at different rates as the cylinder-wall gap varies.

I.2. Wall Normal Motion

Wall normal motion takes a different non-dimensional lubrication scaling relationships due to the reference velocity taken in the wall normal direction. The velocity and pressure terms take the following form in the wall normal direction,

$$u = \sqrt{2}\varepsilon^{-1/2} V U, \qquad w = VW, \qquad p = \frac{2\eta V}{r\varepsilon^2} P.$$

Introducing the above non-dimensional terms into Eq. S2 yields the following equation,

$$F_x = \int_{-\infty}^{\infty} \left(-4\eta V \varepsilon^{-1} X P + 4\eta \varepsilon^{-1/2} V X \frac{\partial U}{\partial X}\right) - \eta\left(2\varepsilon^{-1} V \frac{\partial U}{\partial Z} + V\frac{\partial W}{\partial X}\right)\mathrm{d}X. \tag{S10}$$

Gathering the leading order terms of ε gives the force along the x-axis,

$$F_x = -2\eta V \varepsilon^{-1} \int_{-\infty}^{\infty} 2XP + \frac{\partial U}{\partial Z}\mathrm{d}X. \tag{S11}$$

The only difference from the wall parallel and rotation x-axis forcing, Eq. S5, is a higher power of ε and a factor of $\sqrt{2}$. The force in the z direction obtains the following form,

$$F_z = \int_{-\infty}^{\infty} 2\sqrt{2}\eta V \varepsilon^{-3/2} P - 2\sqrt{2}\eta V \varepsilon^{-1/2}\frac{\partial W}{\partial Z} + \eta V\left(2\sqrt{2}\varepsilon^{-1/2}\frac{\partial U}{\partial Z} + \sqrt{2}\varepsilon^{1/2}\frac{\partial W}{\partial X}\right)\mathrm{d}X. \tag{S12}$$

The leading order equation in ε is,

$$F_z = 2\sqrt{2}\eta V \varepsilon^{-3/2} \int_{-\infty}^{\infty} P \mathrm{d}X. \tag{S13}$$

The force in the z direction for the wall normal motion has the largest power of ε with $\alpha = -3/2$. Following the same procedure the wall normal motion generates a torque,

$$T = r\int_{-\infty}^{\infty} 4\eta V \frac{\partial U}{\partial Z} - \eta\left(2V\varepsilon^{-1}\frac{\partial U}{\partial Z} + V\frac{\partial W}{\partial X}\right) - 4\eta V\frac{\partial W}{\partial Z} + \eta V X^2\left(4\frac{\partial U}{\partial Z} + 2\varepsilon\frac{\partial W}{\partial X}\right)\mathrm{d}X. \tag{S14}$$

Gathering the leading order terms of ε produces the torque equation,

$$T = -2\eta r V \varepsilon^{-1} \int_{-\infty}^{\infty} \frac{\partial U}{\partial Z} dX. \tag{S15}$$

The complete description of the forces and torques outlined thus far require solutions for the pressure and velocity fields provided in the following section.

TABLE S1: Reynolds equation boundary conditions

	$U(X,H)$	$U(X<0,0)$	$U(X>0,0)$	$W(X,H)$	$W(X,0)$	$P(\pm\infty)$
$V^{\parallel}$	1	$L\partial_Z U$	0	0	0	0
$V^{\perp}$	0	$L\partial_Z U$	0	1	0	0
Ω	1	$L\partial_Z U$	0	$2X$	0	0

II. SOLUTIONS TO REYNOLDS EQUATIONS

The pressure and velocity solutions are obtained by solving the Reynolds equation introduced in the main text as Eq. 2. The Reynolds equation can be solved subject to three sets of boundary conditions corresponding to the three modes of motion. The boundary conditions for the inhomogeneous slip wall and motion combinations are summarized in Table S1. Reynolds equation solutions are obtained through first integrating the velocity, U. Then applying the boundary conditions gives relationships for U as functions of geometry, H, and pressure, P. Next the continuity equation can be used to close the problem yielding an expression for pressure. As discussed in the main text the domain is split into two segments, $X<0$ and $X>0$, due to the variation in wall slip length. Therefore for every case there are two Reynolds equations that need to be solved. Lastly remaining unknown integration constants are obtained by matching the left and right domain pressure solution and mass flux at $X=0$. The solutions to the pressure and velocity fields at the the cylinder surface allow for the evaluation of the integrals in Eqs. S5, S7, S9, S11, S13, and S15, producing the desired resistance coefficients. The resistance matrix of Eq. 1 is presented here in a slightly different form with ε factored out so that the R_{ii} represents the evaluation of the integral and constant,

$$\begin{bmatrix} F_x \\ F_z \\ T \end{bmatrix} = -\eta \begin{bmatrix} \varepsilon^{-1/2}R_{11} & -\varepsilon^{-1}R_{12} & r\varepsilon^{-1/2}R_{13} \\ -\varepsilon^{-1}R_{21} & \varepsilon^{-3/2}R_{22} & -r\varepsilon^{-1}R_{23} \\ r\varepsilon^{-1/2}R_{31} & -r\varepsilon^{-1}R_{32} & r^2\varepsilon^{-1/2}R_{33} \end{bmatrix} \begin{bmatrix} V^{\parallel} \\ V^{\perp} \\ \Omega \end{bmatrix}. \tag{S16}$$

We now present the result of all nine resistance coefficient integrals. Starting with the wall parallel motion which produces the following resistance coefficients:

$$R_{11} = \sqrt{2}\int_{-\infty}^{\infty} 2XP + \frac{\partial U}{\partial Z}dX = \frac{4\sqrt{2}\left(-1+\sqrt{\frac{1}{1+4L}}+L\left(-1+3\sqrt{\frac{1}{1+4L}}+L\left(3+5\sqrt{\frac{1}{1+4L}}\right)\right)\right)\pi}{-1+\sqrt{\frac{1}{1+4L}}+2L(1+5L)}, \tag{S17}$$

$$R_{21} = 2\int_{-\infty}^{\infty} PdX = \frac{3\left(4L\left(1+3L+\sqrt{\frac{1}{1+4L}}\right)-(2+5L)\ln(1+4L)\right)}{-1+\sqrt{\frac{1}{1+4L}}+2L(1+5L)}, \tag{S18}$$

$$R_{31} = \sqrt{2}\int_{-\infty}^{\infty} \frac{\partial U}{\partial Z}dX = \frac{2\sqrt{2}\left(1-\sqrt{\frac{1}{1+4L}}+L\left(3+L-5\sqrt{\frac{1}{1+4L}}-5L\sqrt{\frac{1}{1+4L}}\right)\right)\pi}{-1+\sqrt{\frac{1}{1+4L}}+2L(1+5L)}. \tag{S19}$$

In the limit of $L\to 0$ one obtains the classic solution of Jeffrey [1]: $R_{11}=2\sqrt{2}\pi$, $R_{21}=0$, and $R_{31}=0$, and in the other limit as $L\to\infty$: $R_{11}=6\sqrt{2}\pi/5$, $R_{21}=18/5$, and $R_{31}=\sqrt{2}\pi/5$. For the wall normal motion the resistance coefficients are:

$$R_{12} = -2\int_{-\infty}^{\infty} 2XP + \frac{\partial U}{\partial Z}dX = R_{21}, \tag{S20}$$

$$R_{22} = -2\sqrt{2}\int_{-\infty}^{\infty} PdX =$$

$$\frac{\left(\pi^2\sqrt{\frac{1}{1+4L}}(18+36L-132L^2-360L^3)+6\left(-3+2L^2(8+5L(4+5L))\right)\pi^2-9(4L(-1+2L)+\ln(1+4L))^2\right)}{\left(8\sqrt{2}L^2\left(-1+\sqrt{\frac{1}{1+4L}}+2L(1+5L)\right)\pi\right)}, \tag{S21}$$

$$R_{32} = -2\int_{-\infty}^{\infty} \frac{\partial U}{\partial Z}dX = \frac{3\left(4L\left(-3+L-\sqrt{\frac{1}{1+4L}}\right)+(4+5L)\ln(1+4L)\right)}{2\left(-1+\sqrt{\frac{1}{1+4L}}+2L(1+5L)\right)}. \tag{S22}$$

TABLE S2: Reynolds equation boundary conditions Janus cylinder

	$U(X<0,H)$	$U(X>0,H)$	$U(X,0)$	$W(X,H)$	$W(X,0)$	$P(\pm\infty)$
$V^{\parallel}$	1	$L\partial_Z U$	0	0	0	0
$V^{\perp}$	0	$L\partial_Z U$	0	1	0	0
Ω	1	$L\partial_Z U$	0	$2X$	0	0

In the limit of $L \to 0$ one obtains the classic solution of Jeffrey: $R_{12} = 0$, $R_{22} = \frac{3\left(-48+25\pi^2\right)}{20\sqrt{2}\pi}$, and $R_{32} = 0$, in the other limit $L \to \infty$: $R_{12} = 18/5$, $R_{22} = 3\sqrt{2}\pi$, and $R_{32} = 3/5$. Finally for the rotation motion we obtain the following set of resistance coefficients:

$$R_{13} = \sqrt{2}\int_{-\infty}^{\infty} 2XP + \frac{\partial U}{\partial Z} dX = R_{31}, \tag{S23}$$

$$R_{23} = 2\int_{-\infty}^{\infty} P dX = R_{32}, \tag{S24}$$

$$R_{33} = \sqrt{2}\int_{-\infty}^{\infty} \frac{\partial U}{\partial Z} dX = \frac{\sqrt{2}\left(L + 7L\sqrt{\frac{1}{1+4L}} + 4\left(-1+\sqrt{\frac{1}{1+4L}}\right) + L^2\left(17+5\sqrt{\frac{1}{1+4L}}\right)\right)\pi}{-1+\sqrt{\frac{1}{1+4L}}+2L(1+5L)}. \tag{S25}$$

In the limit of $L \to 0$ one obtains the classic solution of Jeffrey: $R_{13} = 0$, $R_{23} = 0$, and $R_{33} = 2\sqrt{2}\pi$, and in the other limit as $L \to \infty$: $R_{13} = \sqrt{2}\pi/5$, $R_{23} = 3/5$, and $R_{33} = 17\sqrt{2}\pi/10$. Equations S17-S25 verify the known symmetry of the resistance coefficient matrix, $R_{12} = R_{21}$, $R_{13} = R_{31}$, and $R_{23} = R_{32}$, reducing the overall resistance matrix to 6 unique terms.

The same process as detailed above can be repeated for the Janus cylinder with the only change being the boundary conditions. The Janus cylinder has slip occurring on the cylinder surface. These boundary conditions are summarized in Table S2. For brevity we summarize the results in the resistance matrix utilizing a transformation matrix relating the Janus cylinder terms to the inhomogeneous wall slip solutions,

$$\begin{bmatrix} \hat{f}_x^{\parallel} \\ \hat{f}_x^{\perp} \\ \hat{f}_x^{\omega} \\ \hat{f}_z^{\perp} \\ \hat{f}_z^{\omega} \\ \hat{t}^{\omega} \end{bmatrix} = \begin{bmatrix} 0&0&0&0&0&1 \\ 0&0&0&0&1&0 \\ 0&0&1&0&0&0 \\ 0&0&0&1&0&0 \\ 0&1&0&0&0&0 \\ 1&0&0&0&0&0 \end{bmatrix} \begin{bmatrix} f_x^{\parallel} \\ f_x^{\perp} \\ f_x^{\omega} \\ f_z^{\perp} \\ f_z^{\omega} \\ t^{\omega} \end{bmatrix}. \tag{S26}$$

We remind the reader that for the Janus cylinder the evaluation of Eqs. S17-S25 will be consistent, but they will be associated with different integrals. For example the Janus cylinder has $\hat{R}_{11} = \sqrt{2}\int_{-\infty}^{\infty} 2XP + \partial_Z U \mathrm{d}X$ which is equal to inhomogeneous wall $R_{33} = \sqrt{2}\int_{-\infty}^{\infty} \partial_Z U \mathrm{d}X$.

III. SCALING LAW DERIVATIONS

In the following we provide additional derivation details of the scaling laws presented in the main text. The Taylor expansion about $L = 0$ for the wall normal lift and drag coefficients for the single transition wall respectively are as follows:

$$f_z^{\parallel} = \varepsilon^{-1}\left(4L - 6L^2 + \frac{107L^3}{10} + \mathcal{O}(L^4)\right), \tag{S27}$$

$$f_z^{\perp} = \varepsilon^{-3/2}\left(-3\left(\sqrt{2}\pi\right) + \frac{9\pi L}{2\sqrt{2}} + \left(\frac{16\sqrt{2}}{\pi} - \frac{45\pi}{4\sqrt{2}}\right)L^2 + \left(-\frac{76\sqrt{2}}{\pi} + \frac{63\pi}{2\sqrt{2}}\right)L^3 + \mathcal{O}(L^4)\right). \tag{S28}$$

The leading order coefficients for lift, $f_z^{\parallel} \approx 4\varepsilon^{-1}L$, and drag, $f_z^{\perp} \approx -3\sqrt{2}\pi\varepsilon^{-3/2}$, are used to set wall normal forces equal and the wall normal displacement is obtained shown in the main text. For the Janus cylinder traveling parallel

to the wall the Taylor expansion leading to Eq. 8 is as follows,

$$\hat{f}_z^{\parallel} = \varepsilon^{-1}\left(2L - 4L^2 + \frac{34L^3}{5} + \mathcal{O}(L^4)\right), \tag{S29}$$

$$\hat{f}_z^{\perp} = \varepsilon^{-3/2}\left(-3\left(\sqrt{2}\pi\right) + \frac{9\pi L}{2\sqrt{2}} + \left(\frac{16\sqrt{2}}{\pi} - \frac{45\pi}{4\sqrt{2}}\right)L^2 + \left(-\frac{76\sqrt{2}}{\pi} + \frac{63\pi}{2\sqrt{2}}\right)L^3 + \mathcal{O}(L^4)\right). \tag{S30}$$

Then we can approximate coefficients for lift as $\hat{f}_z^{\parallel} \approx 2\varepsilon^{-1}L$, and drag as $\hat{f}_z^{\perp} \approx -3\sqrt{2}\pi\varepsilon^{-3/2}$. Balancing the approximate lift and drag forces provides the wall normal displacement estimate (see Table 1 in main paper), which is obtained through neglecting inertial effects of the cylinder.

To elaborate on the importance of the cylinder inertia, we explain here the scaling estimate derivations with cylinder inertia taken into account. The full Newton's equation of motion for cylinder velocity away from the wall can be written as

$$m\frac{dV^{\perp}}{dt} = F_z^{\parallel} + F_z^{\perp}, \tag{S31}$$

where $F_z^{\parallel}$ is the slip-transition induced lift force per unit length, $F_z^{\perp}$ is the standard drag force per unit length and m is cylinder mass per length. If either the cylinder mass or the change of wall-normal velocity is sufficiently small – the latter can occur if the inertial term acts only for a very small interval in time, that is, cylinder accelerates to steady velocity quickly and most of the motion happens in steady, non-inertial regime –, the inertial term can be neglected and the overall wall-normal motion would be governed by the balance of the lift and drag forces, as assumed in the main paper. To understand if we fulfill one of these conditions, we can investigate the initial stage of the motion, where inertia is always important (because there is acceleration) but wall-normal velocity is very small (and thus the drag force is very small). Assuming constant acceleration, we can balance the inertia and lift force

$$m\frac{V^{\perp}}{\tau_a} \sim \eta f_z^{\parallel} V^{\parallel}, \tag{S32}$$

where we have defined the acceleration time scale τ_a over which the particle reaches the steady wall-normal velocity $V^{\perp}$. Assuming that we reach the steady wall-normal velocity $V^{\perp}$ used in the inertia-less assumption $V^{\perp} = V^{\parallel}\Delta/l_c \sim V^{\parallel}l/l_c$ we get the following estimate of the acceleration time scale

$$\tau_a \sim \frac{m}{\eta}\epsilon^{3/2}, \tag{S33}$$

where we have also used the Taylor expansion (S29) of coefficient $f_z^{\parallel}$. Now, recall that the wall-normal motion away from the wall happens over transition time scale $\tau = l_c/V^{\parallel}$, defined in the main paper. In order to be able to neglect the inertial term, we require that the particle accelerates to the steady wall-normal velocity in a time interval much smaller compared to the transition time, i.e., $\tau_a \ll \tau$. This condition can be rewritten as

$$\frac{\tau_a}{\tau} \sim \frac{m\,\varepsilon\,V^{\parallel}}{\eta\,r} := N_\rho \ll 1. \tag{S34}$$

We have validated this condition in our numerical experiments, by considering different density ratios. In Fig. S1 we see that for time scale ratios up to $N_\rho = 0.77$ and density ratios $\rho_c/\rho = 10$ the trajectories of the cylinder are almost indistinguishable. This provides additional confirmation that the numerical experiments provided in the main paper are relevant to density ratios found in biological applications. For example, for red blood cell example we found $N_\rho = 10^{-8}$, which also shows that the red blood cells are expected to follow the non-inertial scaling as derived in the main paper.

Next, following the negligible inertia assumption, we provide the derivation of the scaling laws for cylinder migration due to imposed rotation on neutrally buoyant cylinders. We begin with the inhomogeneous wall. We consider the net migration over one revolution. This provides us with cylinder velocities of $\Omega \sim \pi/\tau$ and $V^{\perp} \sim \Delta/\tau$, where τ is the time scale. The force coefficients are again approximated with a Taylor series expansion around $L = 0$ where the drag is still given by Eq. S28 and the lift is given as,

$$f_z^{\omega} = \varepsilon^{-1}\left(2L - 4L^2 + \frac{34L^3}{5} + \mathcal{O}(L^4)\right). \tag{S35}$$

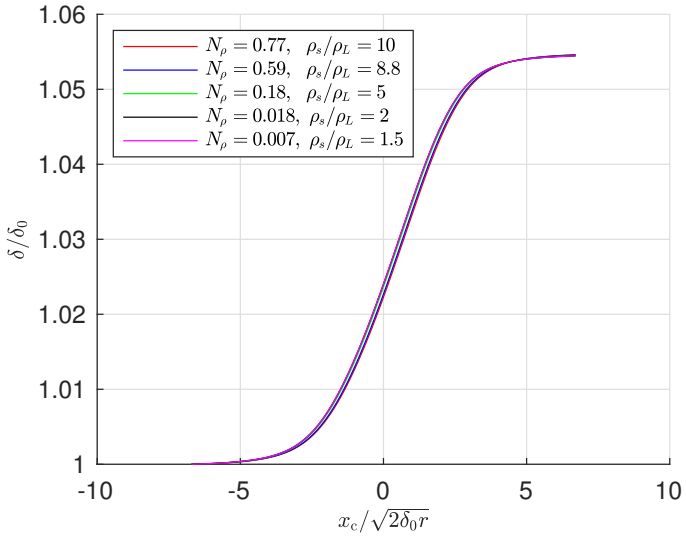

FIG. S1: Wall normal displacements as a function of transverse position for several cylinder densities. We can observe no discernible difference in the trajectory and in the final displacement for the range of densities presented in agreement with the condition on N_ρ.

This produces the leading order estimates as $f_z^\omega \approx 2\varepsilon^{-1}L$ and $f_z^\perp \approx -3\sqrt{2}\pi\varepsilon^{-3/2}$. Then setting $f_z^\omega \eta r\Omega = f_z^\perp \eta V^\perp$ provides us with the scaling relationship for one revolution of a neutrally buoyant smooth cylinder above a inhomogeneous wall as,

$$\Delta \sim \ell\sqrt{\frac{r}{\delta}}. \tag{S36}$$

To obtain a similar argument for how the Janus cylinder migrates away from the wall requires a slightly different approach as the force acting on the Janus cylinder will vary drastically as the cylinder rotates. We consider a simplification where migration is modeled in two steps; away from the wall for half a revolution followed by motion towards the wall for the second half of the revolution. In this way we maintain a similar approach as the smooth cylinder rotation. We use the same velocity definitions as above. Starting with the Taylor expansion about $L = 0$ we have the same drag coefficient as before Eq. S30 and the lift coefficient as,

$$\hat{f}_z^\omega = \varepsilon^{-1}\left(4L - 6L^2 + \frac{107L^3}{10} + \mathcal{O}(L^4)\right). \tag{S37}$$

Thus the leading order approximation is $\hat{f}_z^\omega \approx 4\varepsilon^{-1}L$ and the drag is still $\hat{f}_z^\perp \approx -3\sqrt{2}\pi\varepsilon^{-3/2}$. Setting $\hat{f}_z^\omega \eta r\Omega = \hat{f}_z^\perp \eta V^\perp$ gives the displacement during the first half of the revolution,

$$\Delta_1 \sim \delta_0^{-1/2} r^{1/2}\ell. \tag{S38}$$

The second half of the revolution will follow the same derivation with a new gap, δ_1, which will be larger than δ_0. The wall normal force will now be towards the wall. Thus the net migration will be the summation of both displacements,

$$\Delta_1 + \Delta_2 = \delta_0^{-1/2} r^{1/2}\ell - \delta_1^{-1/2} r^{1/2}\ell. \tag{S39}$$

Replacing $\delta_1 = \delta_0 + \Delta_1$ and some rearranging one obtains the wall normal displacement scaling,

$$\Delta \sim \ell\sqrt{\frac{r}{\delta_0}} - \frac{\ell\sqrt{\frac{r}{\delta_0}}}{\sqrt{1 + \ell r^{1/2}\delta_0^{-3/2}}}. \tag{S40}$$

IV. SCALING LAW CORRECTION FOR PATTERN WALL

The simple scaling for the single transition proposed in the main paper, $\Delta \sim \ell$, is insufficient to explain the net migration away from a patterned wall. This scaling implies equal amount of upwards displacement for slip no-slip

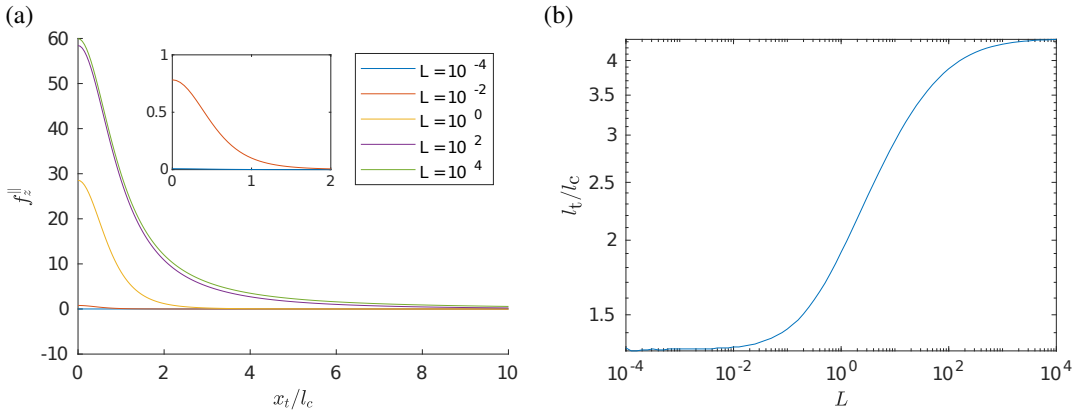

FIG. S2: (a) The non-dimensional lift force as a function of distance from the surface transition point (x_t). For non-dimensional slip length $L < 10^{-2}$ the standard definition for contact length (l_c) is a reasonable approximation (highlighted with the inset). For larger slip lengths the force is non-negligible with $x_\mathrm{t}/l_\mathrm{c} > 1$. (b) Transition length as a function of non-dimensional slip length as defined in Eq. S41.

transition as the preceding downwards displacement for no-slip slip transition. In reality the migration could be a result of a more complex coupling between forces and effective time over which they act. This effect could be captured by modifying the length scale over which the the lift force approximately acts, see main paper Eq. 7. Here we call this length scale as "transition length". This would in turn for the same translation velocity modify the effective time over which the lift force is approximately acting on the cylinder. This modification is motivated by analytic solution of the lift coefficient configuration, where the cylinder center is moved away from the transition point. In Fig. S2(a) we show results for various dimensionless slip length $L = \ell/\delta_0$ values. It is evident that as L changes, the transition length also changes. If physical slip length ℓ is kept constant, as for the patterned wall considered in the main paper, the L value decreases if gap thickness δ_0 is increased. Consequently the transition length shrinks when the cylinder is pushed away during the preceding slip no-slip transition, leading to smaller displacement towards the wall over next transition, even if the effective force is similar.

We define the transition length with a help of the integral quantity,

$$l_\mathrm{t} = \frac{l_\mathrm{c}}{f_z^{\parallel,max}} \int_{-\infty}^{\infty} f_z^{\parallel}\, \mathrm{d}X, \tag{S41}$$

where $f_z^{\parallel,max}$ is the maximum value of the lift force obtained when the cylinder is directly above the transition point. This integral measure provides an estimate of an effective length over which a constant maximal force could be expected to apply for capturing the displacement in the wall normal direction. Figure S2(b) shows l_t as a function of L in a log-log plot. From this figure one can obtain a power law relationship, $l_\mathrm{t} = l_\mathrm{c} L^{\beta}$. Considering small L one obtains $\beta \approx 0.003$ suggesting only a minor modification to the original scaling is required to capture the more complex patterned wall dynamics. With the new transition length the displacement estimate for a single slippage transition is modified as follows. As in the main paper, we estimate cylinder velocities as $V^{\parallel} \sim l_\mathrm{t}/\tau$ and $V^{\perp} \sim \Delta/\tau$, where τ is the time scale. We take the leading order terms in Eqs. S27 and S28 and setting the wall normal forces equal $f_z^{\parallel}\eta V^{\parallel} = f_z^{\perp}\eta V^{\perp}$. This gives the scale estimate for migration of a cylinder over one surface transition as,

$$\Delta \sim \delta_0^{-0.003}\ell^{1.003}. \tag{S42}$$

This scaling estimate predicts a smaller displacement for a larger gap thickness δ_0 and is consequently in agreement with net migration away from the wall.

V. NUMERICAL METHOD

A finite element solver (FreeFem++) is used for the numerical component of this research [2]. We use quadratic elements for the velocity components, u, w and linear elements for pressure, p. Stokes equations are solved coupled with an Euler forward time stepping scheme. At each time step Newton's equations are solved for the cylinder velocity, $\boldsymbol{V}$ and rotation Ω, from

$$\rho_\mathrm{c} V_\mathrm{c} \frac{\mathrm{d}\boldsymbol{V}}{\mathrm{d}t} = \int_S \boldsymbol{\sigma}\cdot\boldsymbol{n}\mathrm{d}S + V_\mathrm{c}\left(\rho_\mathrm{c} - \rho\right)\boldsymbol{g}, \tag{S43}$$

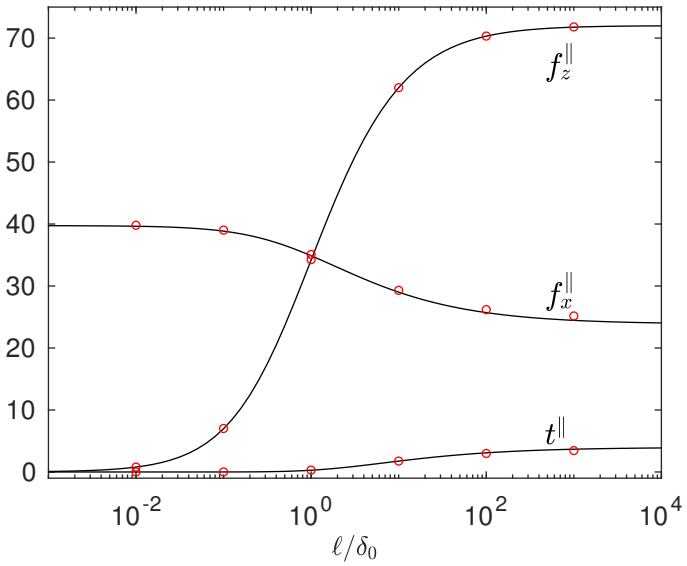

FIG. S3: Comparison of the analytical force coefficients for wall parallel motion to FEM simulations. Here analytical solutions are shown in black and FEM simulations are shown with red circles.

and

$$r\rho_{\mathrm{c}} I_{\mathrm{c}} \frac{\mathrm{d}\Omega}{\mathrm{d}t} = \int_S \boldsymbol{r} \times (\boldsymbol{\sigma} \cdot \boldsymbol{n}) \, \mathrm{d}S. \tag{S44}$$

The following values are used in the numerical simulation; fluid density $\rho = 970\,\mathrm{kg{\cdot}m^{-3}}$, fluid viscosity $\eta = 1\,\mathrm{Pa{\cdot}s}$, particle density $\rho_c = 8510\,\mathrm{kg{\cdot}m^{-3}}$, particle diameter $d = 0.0127\,\mathrm{m}$, volume per length $V_c = 1.13 \times 10^{-3}\,\mathrm{m}^2$, second moment of inertia per length $I_c = 1.73 \times 10^{-5}\,\mathrm{m}^3$. The computational domain is re-meshed after each time step. The domain has stress-free boundary conditions for the fluid-fluid boundaries, Dirichlet conditions for the no-slip surfaces and Neumann conditions for the slip surfaces. The mesh is defined to maintain a minimum number of elements between the particle and wall to ensure good resolution of the thin gap. A mesh convergence test was performed increasing the minimum number of elements in the gap from 12 to 16 produced a relative change in pressure on the order of 10^{-5} suggesting a sufficiently converged solution. Finally, in Fig. S3, we compare the resistance coefficients obtained through FEM simulations with the analytical solutions, where we observe a good agreement (2% relative error), over a large range of slip lengths. The other resistance matrix components have comparable agreement.

[1] D. Jeffery and Y. Onishi, Q. J. Mech. Appl. Math. **34**, 129 (1981).
[2] F. Hecht, J. Numer. Math. **20**, 251 (2012).